ELSEVIER

Materials Science and Engineering A304–306 (2001) 992–996

MATERIALS SCIENCE & ENGINEERING A

www.elsevier.com/locate/msea

Thermodynamic and magnetic properties of multicomponent $(Fe, Ni)_{70}Zr_{10}B_{20}$ amorphous alloy powders made by mechanical alloying

Y.J. Liu [a,*], I.T.H. Chang [a], M.R. Lees [b]

[a] *School of Metallurgy and Materials, The University of Birmingham, Edgbaston, Birmingham B15 2TT, UK*
[b] *Department of Physics, The University of Warwick, Coventry CV47 7AL, UK*

Abstract

The correlation between the thermodynamic and magnetic properties of mechanically alloyed (MAed) $(Fe_{1-x}Ni_x)_{70}Zr_{10}B_{20}$ (x = 0.1–0.4) amorphous alloy powders was investigated. The activation energy (E_a) for primary crystallization of the b.c.c. α-Fe phase decreased significantly from 356.7 to 139.7 kJ/mol with increasing Ni/Fe ratio from 0.11 to 0.43 and then increased to 304 kJ/mol for the alloy with a Ni/Fe ratio of 0.67. The Curie temperatures of the $(Fe_{1-x}Ni_x)_{70}Zr_{10}B_{20}$ (x = 0.1–0.4) alloy powders milled at 18 h were found to be in the range 425–625 K. The room temperature coercivity of the as-milled amorphous powders was in the range 37–44 G. However, they were dramatically reduced to values in the range 11–24 G after annealing at temperatures from 250 to 575 K. The minimum coercivities obtained after in situ annealing of amorphous powder were 8 G for $(Fe_{0.6}Ni_{0.4})_{70}Zr_{10}B_{20}$ and 10 G for $(Fe_{0.8}Ni_{0.2})_{70}Zr_{10}B_{20}$, respectively.

Keywords: Activation energy; Magnetic properties; Mechanical alloying

1. Introduction

Melt-spun Fe-based amorphous materials have already been recognized as good soft magnetic materials. Recently, more and more attention has been paid to the mechanically alloyed Fe-based soft magnetic material, especially nanostructured Fe–Co and Fe–Zr–B–Cu alloy systems [1–3]. It was found that the coercivity for mechanically alloyed (MAed) nanocrystalline alloy powders is much higher than that of traditional melt-spun soft magnetic materials.

The amorphous phase in $(FeCoNi)_{70}Zr_{10}B_{20}$ alloy systems can be obtained by a mechanical alloying process [4]. The influences of annealing temperature and alloy composition on the magnetic properties for this alloy system are still unclear. In this paper, we discuss the effects of annealing temperature on the magnetization and coercivities of amorphous alloy powders. In addition, the effects of alloy composition on the Curie temperatures and minimum coercivities are presented in this paper. Finally, a correlation between the activation energy, magnetization and phase transformation is established.

* Corresponding author. Present address: Department of Materials Engineering, University of Wales, Swansea, Singleton Park, Swansea, SA2 8pp, UK. Fax: +44-1792-295244.
E-mail address: Y.J.Liu@Swan.ac.uk (Y.J. Liu).

2. Experimental methods

Amorphous alloy powders were obtained by mechanical alloying of the elemental or pre-alloyed crystalline powders [4]. Differential scanning calorimetry (Perkin Elmer, Pyris 1) was used to anneal the amorphous powders at different heating rates in order to use Kissinger [5] analysis to determine the apparent activation energies of the crystallization reactions. Pendulum and vibrating sample magnetometers (VSM) (Oxford Maglab) were used to obtain the magnetization and coercivities for a variety of amorphous alloy powders as a function of annealing temperature.

3. Results and discussions

3.1. Activation energy for crystallization reaction

The crystallization of the MAed multicomponent $(Fe_{1-x-y}Co_yNi_x)_{70}Zr_{10}B_{20}$ (x = 0.1–0.4, y = 0, 0.1, 0.3) amorphous alloy powders involved a two-stage process: (1) the formation of b.c.c. α-Fe followed by (2) the formation of other crystalline phases, such as $(Fe, Ni)_{23}B_6$ and f.c.c. γ-FeNi [14]. The activation energies for these two crystallization reactions can be determined by Kissinger [5] analysis.

Kissinger analysis gives the following equation:

$$\mathrm{Ln}\left(\frac{s}{T^2}\right) = -\frac{E_a}{RT} + \text{constant} \quad (1)$$

0921-5093/01/$ – see front matter
PII: S0921-5093(00)01613-0

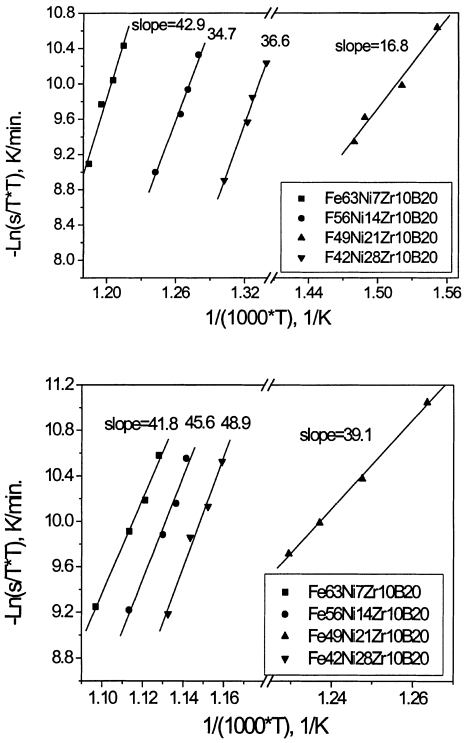

Fig. 1. Kissinger plots for the peak temperature (T_{p1}) of primary crystallization of b.c.c. α-Fe and the peak temperature (T_{p2}) for the formation of complex compounds, respectively.

where s is the heating rate, T the specific temperature, being T_{p1} (the peak temperature for the formation of b.c.c. α-Fe) and T_{p2} (the peak temperature for the formation of other crystalline phases) in this paper, E_a the apparent activation energy and R the gas constant. Fig. 1 shows graphs of $\mathrm{Ln}(s/T^2)$ against $1/T$ for the peak temperature (T_{p1}, the formation of b.c.c. α-Fe) and the peak temperature (T_{p2}, the formation of other crystalline phases) in DSC traces.

The activation energies for the primary crystallization of the b.c.c. α-Fe phase and the formation of the complex compounds are listed in Table 1. The activation energy for the primary crystallization is the main concern in this paper and it is maximum for the alloy with a composition of $Fe_{63}Ni_7Zr_{10}B_{20}$ (356.7 kJ/mol) and minimum for $Fe_{49}Ni_{21}Zr_{10}B_{20}$ alloy (139.7 kJ/mol). The typical activation energies for primary crystallization for Fe-based amorphous alloys were found to be around 300 kJ/mol which includes the contributions from both nucleation and grain growth [6–8]. The activation energy for pure grain growth in nanostructured Fe was determined by Malow and Koch [9] to be 178 kJ/mol. Therefore, in this study, the activation energy for primary crystallization for the alloy of $Fe_{49}Ni_{21}Zr_{10}B_{20}$ is only comparable to the grain growth case. According to a previous study [4], there is a considerable fraction of possible nanocrystals in MAed $Fe_{49}Ni_{21}Zr_{10}B_{20}$ amorphous matrix. Therefore, the activation energy for crystallization is strongly dependent on the degree of amorphous phase (e.g. fraction of crystalline phase in the amorphous matrix) and is significantly reduced where there exists a high degree of nanostructured crystalline phases in the amorphous matrix. This suggests that the other three types of MAed alloy powders appeared to be free of detectable crystalline phase in the amorphous matrix. The degree of amorphous phase in this study has also been detected by measuring the magnetic moment as a function of annealing temperatures.

3.2. Annealing temperature dependence of magnetization

Fig. 2 shows plots of the magnetization (M) of amorphous alloy powders milled for 18 h as a function of annealing temperature. It shows that the ferromagnetic–paramagnetic transition gives a good indication of the phase transformation

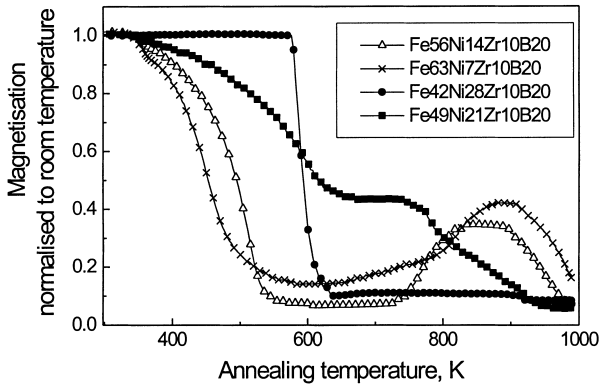

Fig. 2. Normalized magnetization as a function of annealing temperature for all amorphous alloy powders milled for 18 h. The magnetization was normalized to the value at room temperature. This data was collected using a Pendulum magnetometer in an applied field of 2500 Oe.

Table 1
Activation energies for the primary crystallization of b.c.c. α-Fe and the formation of complex compounds, respectively, for all MAed amorphous alloy powders milled for 18 h

Alloys	Slopes for Kissinger plots		Activation energy (kJ/mol)	
	Primary crystallization of b.c.c. α-Fe	Formation of complex compounds	Primary crystallization of b.c.c. α-Fe	Formation of complex compounds
$Fe_{63}Ni_7Zr_{10}B_{20}$	42.9	41.8	356.7	347.5
$Fe_{56}Ni_{14}Zr_{10}B_{20}$	34.7	45.6	288.5	379.1
$Fe_{49}Ni_{21}Zr_{10}B_{20}$	16.8	39.1	139.7	325.1
$Fe_{42}Ni_{28}Zr_{10}B_{20}$	36.6	48.9	304.3	406.6

which occurs during the annealing process of the amorphous alloy powders. Generally, the amorphous phase has a lower Curie temperature (T_c) than the corresponding crystalline phase. The b.c.c. α-Fe phase is ferromagnetic phase. The broad ferromagnetic–paramagnetic transition in the magnetization vs. temperature plot usually indicates the presence of chemical inhomogeneity [10]. When the amorphous alloy powders were heated up to the Curie temperature, there is a significant drop in the magnetization as the ferromagnetic amorphous phase is changed to the paramagnetic amorphous phase if the Curie point is below the crystallization temperature. In this study, the crystallization temperatures for $Fe_{56}Ni_{14}Zr_{10}B_{20}$ and $Fe_{63}Ni_7Zr_{10}B_{20}$ amorphous alloy powders are 600.6 and 579.1 K, respectively [4]. The Curie temperatures of the amorphous phases can be determined from Fig. 2 to be 495 and 425 K for $Fe_{56}Ni_{14}Zr_{10}B_{20}$ and $Fe_{63}Ni_7Zr_{10}B_{20}$ alloy powders, respectively. The temperature window between the crystallization temperature and the Curie points for $Fe_{56}Ni_{14}Zr_{10}B_{20}$ and $Fe_{63}Ni_7Zr_{10}B_{20}$ amorphous alloy powders can be seen to be 105 and 154 K, respectively. When the annealing temperature reaches the crystallization temperature of the amorphous phase, the formation of ferromagnetic crystalline b.c.c. α-Fe phase makes a contribution to the magnetization of the annealed sample and the magnetization increases with increasing annealing temperature. This was caused by the gradual increase in the volume fraction of ferromagnetic b.c.c. α-Fe phase precipitated from the remaining paramagnetic amorphous matrix. A further increase in annealing temperature accelerated the crystallization rate and eventually a maximum magnetization is reached reflecting a saturation in the formation of the b.c.c. α-Fe phase. Subsequently, a paramagnetic drop in magnetization appears when the annealing temperature reaches the Curie point of crystallized b.c.c. α-Fe phase and the material becomes paramagnetic. Hence, a broad peak appears in the plot of magnetization against annealing temperature for $Fe_{56}Ni_{14}Zr_{10}B_{20}$ and $Fe_{63}Ni_7Zr_{10}B_{20}$ amorphous alloy powders.

For $Fe_{42}Ni_{28}Zr_{10}B_{20}$ MAed alloy powders, the Curie point for the amorphous phase of this alloy is around 600 K, which is slightly lower than the crystallization temperature of 619 K. However, there is only slight increase in magnetization above 600 K. This might be due to the smaller volume fraction of crystallized b.c.c. α-Fe phase and the primary f.c.c. γ-Fe Ni phase compared to that for $Fe_{56}Ni_{14}Zr_{10}B_{20}$ and $Fe_{63}Ni_7Zr_{10}B_{20}$ alloy powders. This is confirmed by a further XRD analysis [14].

For MAed $Fe_{49}Ni_{21}Zr_{10}B_{20}$ alloy powders, a different result is seen as shown in Fig. 2. As the annealing temperature increased, an initial decrease in magnetization occurred in the temperature range from room temperature to 650 K. This is then followed by a second decrease in magnetization at a higher temperature (>750 K). This two-step change in magnetization reflects the fact that two ferromagnetic phases exist in the alloy powders. The first ferro–paramagnetic transition indicates the Curie temperature of the amorphous phase in this as-milled alloy powder is about 625 K, which is slightly higher than its crystallization temperature of 611 K. The decrease in magnetization at the first step was found to be less distinct as compared to other three amorphous alloys. This might be due to the chemical inhomogeneity in this alloy powder. The second ferro–paramagnetic transition is associated with the formation of ferromagnetic b.c.c. α-Fe phase from the amorphous matrix. Since the Curie point of amorphous phase is higher than its crystallization temperature for this alloy, the crystallization started before the amorphous phase had reached its Curie point. This results in a saturated value in magnetization in the temperature range from 650 to 750 K. This has been further confirmed by in situ heating in a higher resolution VSM as shown in Fig. 3. It can be seen that on heating the $Fe_{49}Ni_{14}Zr_{10}B_{20}$ alloy powder milled for 18 h there is a rapid increase in the magnetic moment that occurs above 650 K after the initial drop in magnetization of the amorphous phase. The Curie temperature is about 625 K which is in good agreement with that obtained using the Pendulum magnetometer. The high magnetic moment of the $Fe_{49}Ni_{21}Zr_{10}B_{20}$ alloy powder at around 650 K suggested that the crystallization of the b.c.c. α-Fe phase had taken place earlier. The first increase in magnetic moment for alloy powders milled for 18 h in the temperature range 300–500 K might be due to the decrease of free volume or some increase of short-range order. This was also found in other ferromagnetic amorphous alloy systems [11]. In addition, the increase in magnetic moment above 650 K suggests that crystallization of the amorphous phase produces a ferromagnetic phase which was identified by XRD analysis as b.c.c. α-Fe phase. Therefore, the change of magnetization against annealing temperature for the $Fe_{49}Ni_{21}Zr_{10}B_{20}$ alloy powders milled for 18 h indicates the presence of the amorphous phase in this as-milled alloy powder. The chemical inhomogeneity in this amorphous matrix made a contribution to the low activation energy for the crystallization.

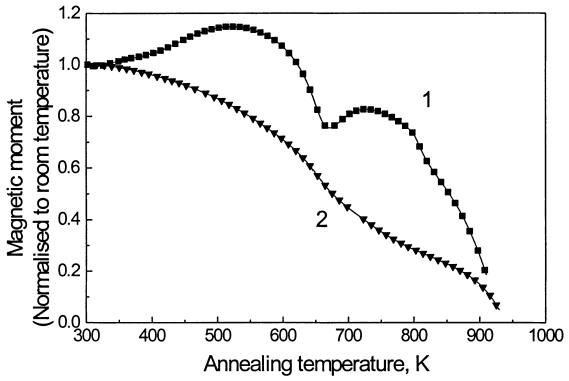

Fig. 3. Annealing temperature dependence of magnetization by in situ annealing of $Fe_{49}Ni_{21}Zr_{10}B_{20}$ alloy powder milled for 18 h. (1) Heating trace for as-milled alloy powders; (2) Cooling trace for the same powder sample having already been crystallized in the heating trace.

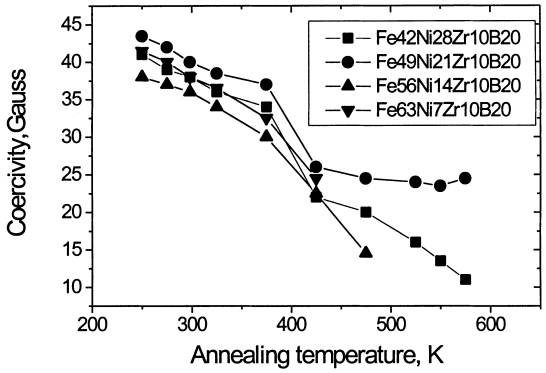

Fig. 4. Annealing temperature dependence of the coercivities for all the amorphous alloy powders milled for 18 h.

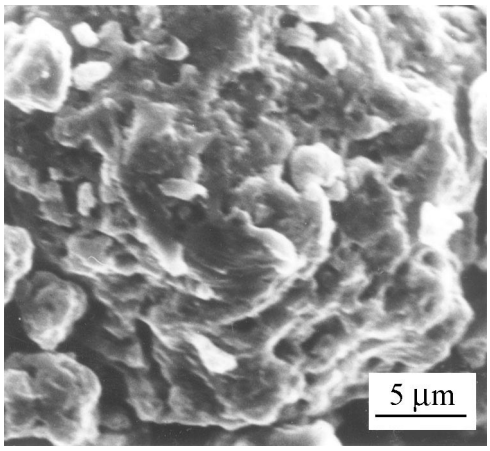

Fig. 5. A typical surface topograph of MAed amorphous alloy powders produced by repeated deformation, welding, and fracturing process.

3.3. Annealing temperature dependence of coercivities (Hci)

In situ measurement of the coercivities (Hci) were performed in a VSM during the annealing process. The annealing temperatures were kept below the Curie points for each amorphous alloy powder since the shape of *M–H* loops changed dramatically above the Curie point. Fig. 4 shows that the coercivities of the as-milled alloy powders decreased with increasing annealing temperatures for all the amorphous alloy powders. Moreover, it can be seen that Hci values for all amorphous alloy powders are much higher than those for the conventional melt-spun soft magnetic amorphous materials. $Fe_{49}Ni_{21}Zr_{10}B_{20}$ has the highest Hci values whereas the Hci values for $Fe_{56}Ni_{14}Zr_{10}B_{20}$ are the lowest.

The high Hci values for all MAed amorphous alloy powders might be due in part to the special microstructure in the as-milled powder. In contrast to the melt-spun metallic amorphous alloy, during mechanically alloying, the alloy powders experience a repeated cold deformation, welding, fracturing process. A typical surface topograph of powders for all the MAed alloys used in this study can be seen in Fig. 5. The powder has a "cabbage structure" as seen by Schafer et al. [2] in MAed Fe–Zr–B–Cu nanocrystalline powder. It was found that such a cabbage structure caused a corresponding cabbage-like magnetic domain pattern and that a long-range stress anisotropy existed in the as-milled powder particle. This produced a high coercivity in mechanically alloyed particles. In addition, the welded interface between different layers could act as pinning sites for domain walls or interrupt exchange coupling in the radial direction of the particle. This might be one of the reasons for the relatively high coercivity in the MAed amorphous alloy powder as observed in the present study. Even for melt-spun $Fe_{40}Ni_{40}P_{14}B_6$ amorphous alloy, the coercive force increased from 0.01 Oe before cold rolling to 20 Oe after 40% cold rolling [12].

The high coercivity of as-milled amorphous alloy powders may also be a result of chemical inhomogeneity, which might be due to both the nanocrystalline phase in the amorphous matrix and impurities (e.g. Fe and Cr) which came from the milling tools. For instance, the $Fe_{49}Ni_{21}Zr_{10}B_{20}$ alloy powders milled for 18 h consisted of nanocrystalline boron-rich and amorphous phases. The amorphous alloy powders of $Fe_{56}Ni_{14}Zr_{10}B_{20}$, $Fe_{63}Ni_7Zr_{10}B_{20}$ and $Fe_{42}Ni_{28}Zr_{10}B_{20}$ were found to be more homogeneous than the $Fe_{49}Ni_{21}Zr_{10}B_{20}$ alloy powders. Therefore, the coercivities for $Fe_{49}Ni_{21}Zr_{10}B_{20}$ as-milled alloy powders are much higher than the values for the other three amorphous alloys powder.

The detrimental effects on the coercivity resulting from the chemically inhomogeneity cannot be effectively eliminated. However, the effects of heterogeneous deformation anisotropy on coercive force can be significantly reduced for mechanically alloyed powders [1,13]. In the present study, the annealing of the amorphous alloy powders below the Curie temperature reduced the coercivity by as much as 60–80%. An attempt has been made to further decrease the coercivity by annealing the as-milled powders just below the onset of crystallization temperatures. The minimum coercivities obtained after in situ annealing of the amorphous powder were 8 G for $(Fe_{0.6}Ni_{0.4})_{70}Zr_{10}B_{20}$ and 10 G for $(Fe_{0.8}Ni_{0.2})_{70}Zr_{10}B_{20}$, respectively.

4. Conclusions

The activation energy, magnetization, magnetic moment and coercivities for MAed alloy powders are strongly dependent on the degree of amorphous phase present within the as-milled alloy powders. The apparent activation energy for $Fe_{63}Ni_7Zr_{10}B_{20}$, $Fe_{56}Ni_{14}Zr_{10}B_{20}$ and $Fe_{42}Ni_{28}Zr_{10}B_{20}$ amorphous alloy powders are much higher than that for $Fe_{49}Ni_{21}Zr_{10}B_{20}$ alloy powder which consists of nanocrystalline boron-rich phase. Annealing of MAed amorphous alloy powders below the Curie temperature dramatically reduces the coercivities by 60–80%. The nature of the ferromagnetic–paramagnetic transition can give an indication of the chemical homogeneity and the short-range

ordering in the amorphous alloy powders. Low temperature annealing (e.g. below 550 K, close to T_g) of $Fe_{49}Ni_{21}Zr_{10}B_{20}$ alloy powders caused a gradual increase in the magnetic moment between 20 and 30% because of a decrease in the free volume or an increase in the short-range order.

Acknowledgements

The author Y.J. Liu is very grateful for the financial support from the ORS and the School of Metallurgy and Materials of the University of Birmingham. The authors would like to thank Prof. I.R. Harries for the provision of experimental facilities.

References

[1] Ch. Kuhrt, L. Schultz, J. Appl. Phys. 71 (1992) 1897.
[2] R. Schafer, S. Roth, C. Stiller, J. Eckert, U. Klement, L. Schultz, IEEE Trans. Magn. 32 (1996) 4383.
[3] C. Stiller, J. Eckert, S. Roth, R. Schafer, U. Klement, L. Schultz, J. Non-Cryst. Solids 205–207 (1996) 620.
[4] Y.J. Liu, I.T.H. Chang, P. Bowen, in: RQ10 Proceedings, Bangalore, India, 1999.
[5] H.E. Kissinger, Anal. Chem. 29 (1957) 1702.
[6] F.E. Luborsky, Mater. Sci. Eng. 28 (1977) 138.
[7] R.S. de Biasi, M.L.N. Grillo, J. Alloys and Compounds 279 (1998) 233.
[8] Y. Takahara, Mater. Trans. JIM 37 (1996) 1453.
[9] T.R. Malow, C.C. Koch, Mater. Sci. Forum 225 (1996) 595.
[10] S.R. Elliott, in: S.R. Elliott (Ed.), Physics of Amorphous Materials, Longman, New York, 1983, p. 354.
[11] P.R. Ruuskanen, R.B. Schwarz, J.D. Thompson, Phil. Mag. B 69 (1994) 47.
[12] F.E. Luborsky, J.L. Walter, D.G. LeGrand, IEEE Trans. Magn. 12 (1976) 930.
[13] J. Loffler, H.V. Swygenhoven, W. Wagner, Nanostruct. Mater. 9 (1997) 523–526.
[14] Y.J. Liu, Ph.D. Thesis, University of Birmingham, 2000.